DESIGN OF NATURAL LAMINAR FLOW FUSELAGES

D.P. Coiro F. Nicolosi

Università degli Studi di Napoli "Federico II"
Dipartimento di Progettazione Aeronautica
Via Claudio 21 - 80125 Napoli - ITALY

Modern construction techniques in aerodynamic surface construction allow long runs of Natural Laminar Flow (NLF) along fuselages provided that their shape has been properly designed. A numerical optimization iterative procedure for drag reduction by shape modification of axialsymmetric and three-dimensional bodies, has been developed. To this aim we propose a geometric parameterization of a general 3D body. Reduction of drag through an extension of laminar flow runs, for 3D and axialsymmetric bodies, is shown. An investigation of existing transition prediction methods has been done with special regard to their applicability to high Reynolds numbers range. A regrettable lack of experimental data at Reynolds numbers typical of real airplanes is recognized. A modular numerical code developed to perform shape optimization for drag reduction has proven to be efficient and reliable.

List of Symbols

L = body length
A_M = nondimensional maximum frontal area, A_M/L^2
C_D = drag coefficient based on maximum frontal area
U_∞ = frestream velocity
u_e = nondimensional external local velocity, $=U_e/U_\infty$
C_p = pressure coefficient
fr = fineness ratio
f = nondimensional equivalent area, $f=C_D \cdot A_M$
x = nondimensional longitudinal coordinate, =x/L
x_m = nondimensional longitudinal location of maximum thickness, $=x_m/L$
x_{tr} = nondimensional longitudinal coordinate at transition
x_{sep} = nondimensional longitudinal coordinate at turbulent separation
s = nondimensional surface length along body streamline
θ = boundary layer momentum thickness
H = boundary layer shape factor
T-S = Tollmien-Schlichting
n = logarithmic exponent of amplitude-growth ratio of boundary layer disturbances
R_L = Reynolds number based on frestream conditions and body length
R_X = Reynolds number based on frestream conditions and longitudinal coordinate along the body
R_θ = Reynolds number based on frestream conditions and θ
F_{OBJ} = Objective function
y, z = lateral and normal coordinates

Introduction

Present airplane construction techniques result in the production of smooth and accurate aerodynamic surfaces. These surfaces allow for long runs of natural laminar boundary layer flow (NLF), with a resultant drag reduction.

A major portion of the past research for achieving NLF, has been focused on airplane lifting surfaces [1]. However, fuselage shaping to increase natural laminar flow extension has received less attention in the literature, except for sailplane and hydrodynamic bodies.

The importance of fuselage skin-friction drag is well known. It can reach about 70% of the total profile drag when wing and tail surfaces work in laminar flow [2]. It is clear that a significant reduction of the total drag will be obtained through an appropriately shaped fuselage. The importance of the laminar flow area extension on the drag coefficient is shown in tab. 1. Drag coefficients for an axialsymmetric body with fineness ratio of fr=5 are listed for various transition locations.

The present study investigates the possibility of obtaining a fuselage shape with a large extension of laminar flow, not only for axialsymmetric bodies, but also for general three-dimensional configurations.

The main goal of this work is to refine and validate computational methods for the design of axialsymmetric and general 3D bodies with a large extension of natural laminar flow area.

Therefore, a computational iterative optimization procedure to design both low drag axialsymmetric bodies and general 3D aircraft fuselages has been developed.

The design code is based on the numerical optimization technique and is made up of several replaceable modules, each of which addresses and solves a part of the complex problem.
Particular attention has been given to the validity of existing transition prediction methods, especially for high Reynolds number flows for which there is lack of experimental data.

Previous Studies

A comprehensive review of previous research has been made by Dodbele et al. [3].
Many investigations have been conducted, especially concerning under-sea bodies and sailplane configurations. However little experimental data is available for flows characterized by high Reynolds number (based on body length), i.e., for Reynolds number range of $30 \div 70\times10^6$. It seems that the transition from laminar to turbulent flow occurs beyond the point of maximum thickness. This would indicate that the pressure gradient on the forebody of the configuration is the predominant factor in designing the body shape.

x_{tr} (transition location)	C_D*
0.50	0.035
0.40	0.042
0.20	0.052
0.10	0.055

*reference area for C_D calculation was maximum frontal area

Table 1 Drag coefficients for axisymmetric body (fr=5)

Many computational studies have been made in the past for drag reduction of axialsymmetric bodies, which include those done by Zedan and Dalton [4], Parson and Goodson [5].
Dodbele et al.[3] has proposed a method to obtain minimal drag for three-dimensional bodies. The method includes summing up a cambered mean line to an axialsymmetric thickness distribution, which was previously optimized to have minumum drag.
In this work we propose a method [6] to design the optimal shape of a general three-dimensional body, modifying directly the original geometry and investigating the effect of the local curvature variation on pressure distibution, transition and total drag.

Aerodynamic Analysis

The aerodynamic analysis is performed using an inviscid potential field solver coupled with a viscous solver which calculates the boundary layer development along the body.

Axialsymmetric inviscid calculation

We have developed a code based on axial singularity distribution, as proposed by Von Karman [7].
Comparison of the code results with analytical solutions and calculations for some bodies which present a variation of longitudinal curvature, have shown that this method is accurate in predicting pressure distribution on regular bodies (see Fig. 1) but fails for bodies like that shown in fig. 2.
The main advantage of this method is the very low computational cost. This is an attractive feature considering the iterative procedure employed for the shape optimization.
Erratic behaviour of solutions based on axial singularity distribution was also shown by Hess [8].

Three-dimensional inviscid calculation

One way to overcome the problems stressed previously, is to employ a three-dimensional panel code based on surface singularity distribution. Because one of the main goals of the present work is to design, through numerical optimization, general three-dimensional bodies, we developed a 3D numerical code based on surface singularities distribution [9].
To validate our code, we calculated inviscid pressure distribution for several different configurations. For all bodies tested, the code performed well. Comparisons with experimental or other calculated data showed a high level of agreement. (An example is shown in fig. 2).

Boundary layer calculation

An integral axialsymmetric boundary layer method has been coded and used to simulate the effect of viscosity on the external inviscid pressure distribution. The energy equation has been used in conjunction with the Von Karman momentum equation and Drela 2D closure correlations [10] have been coded for both laminar and turbulent parts of the boundary layer.

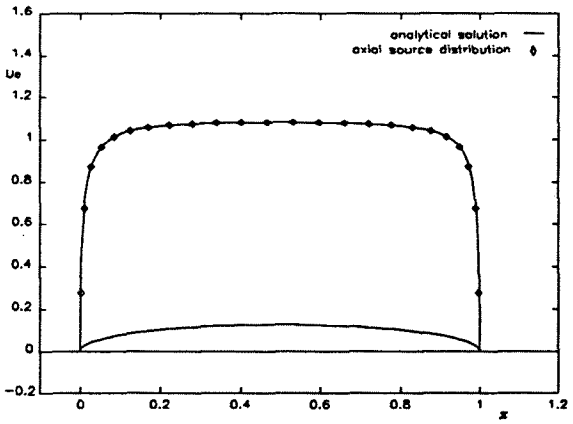

Fig. 1 Comparison of analytical and numerical solution for an ellipsoid of fr=4

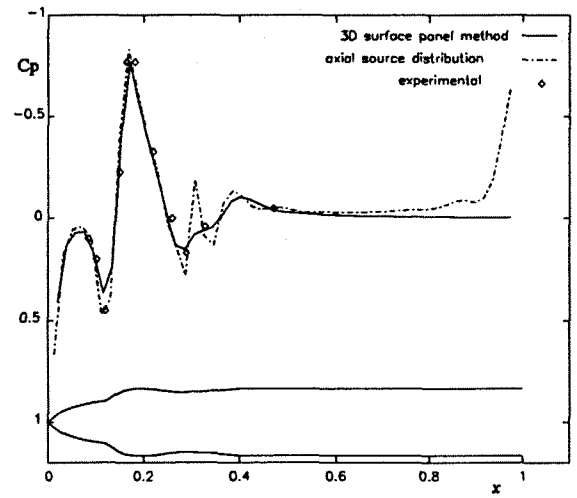

Fig. 2 Comparison of numerical and experimental solution for a spheroid with anular bump

Drag is evaluated with the Young formula [11] which is based on integral quantities of the boundary layer, evaluated at the body's trailing edge.
For general three-dimensional bodies we have calculated the axialsymmetric boundary layer along streamlines contained in the fuselage symmetrical plane (see fig.3). The calculations were obtained from the 3D velocity field, using the radius distribution of an "equivalent axialsymmetric body". This was obtained from the original body by assigning a circular shape (of the same area) to every section.

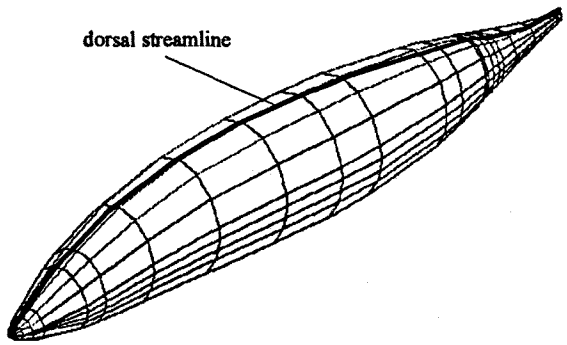

Fig. 3 Dorsal streamline along a fuselage

Transition

Because an accurate prediction of transition onset is a crucial point in designing bodies with large natural laminar flow area, we tested various methods and compared them to experimental results.
The methods used in such a comparison are those of Michel [12], Smith [13], H-Rx [14], Eppler [15] and the e^n method. The e^n method is a result of Van Ingen's work but we used the version proposed by Drela [10].

In particular the n factor is obtained along the streamline using the following expression :

$$n(s) = \int_{s_o}^{s} \frac{dn}{ds}(H,\theta)ds \qquad (1)$$

where s_o is the point where Re_θ assumes its critical value. In general the onset of transition corresponds to a value of n of 9.
The body used for the comparison is a body with a large extent of favourable pressure gradient (fig. 4).

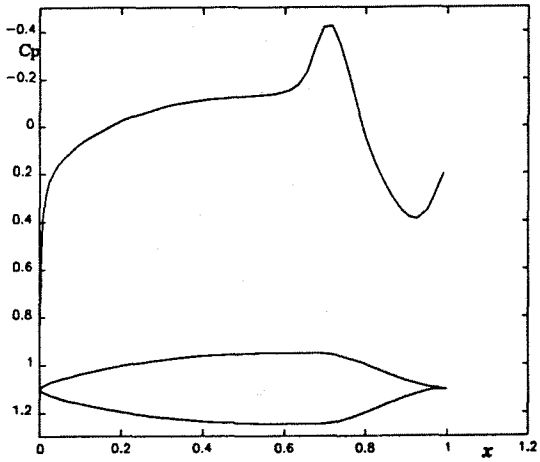

Fig. 4 Pressure distribution and geometry for body of revolution (fr=5)

We tested the different methods at various Reynolds numbers based on total fuselage length. It can be seen from table 2, that at lower Reynolds numbers almost all methods predict transition close to the pressure peak, while for higher values of Reynolds numbers some of them (for example Michel) seem to be insensitive to the increased Reynolds number.

Body of fig. 4 - transition location					
Re_L (million)	Michel	Smith	H-R_x	Eppler	e^n(n=9)
1	.74	.74	.73	.74	.74
4	.74	.74	.73	.73	.74
20	.74	.74	.43	.48	.44
40	.74	.74	.29	.33	.17

Table 2 Transition locations for various methods - body of fig. 4

Fig. 5 shows the influence of Reynolds number on n growth. Fig. 6 shows the development of the boundary layer in terms of Re_x - Re_θ at different values of Reynolds numbers. The same figure represents the transition curve as proposed by Michel. It is clear that at higher Reynolds numbers such a method does not work well because it predicts transition only if adverse pressure gradients are present, independently from the Reynolds number value.

It should be noted that there is a lack of experimental data regarding the transition onset at high Reynolds numbers. In general we can say that at those numbers there is a strong influence of external streamline curvature on transition onset.
Furthermore, we are assuming that transition occurs always for spatial growth of T-S disturbances.
In general and especially for general three-dimensional configurations, the instabilities due to crossflow effect should be monitored.
Obviously to have an accurate transition prediction, a linear stability analysis of laminar boundary layer velocity profile, should be performed. However, this is impratical especially for an iterative design process because of the long computational time needed to do such an analysis.

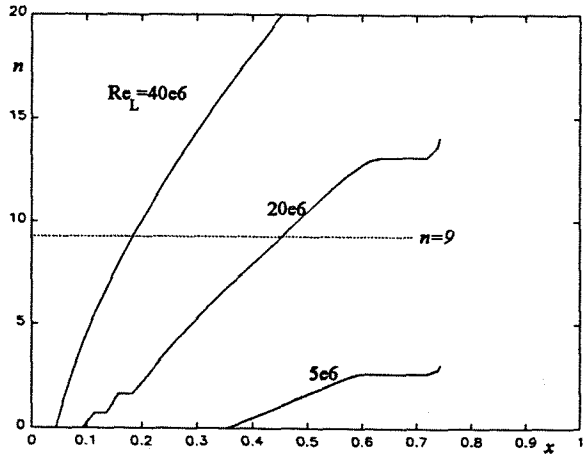

Fig. 5 Logarithmic disturbances amplification factor growth for body of fig. 4 at various Reynolds number

The prediction of transition onset is particularly difficult for bodies characterized by a high fineness ratio because the pressure distribution is almost flat for a large part of the streamline, leading to an uncertainty in the predicted transition point.

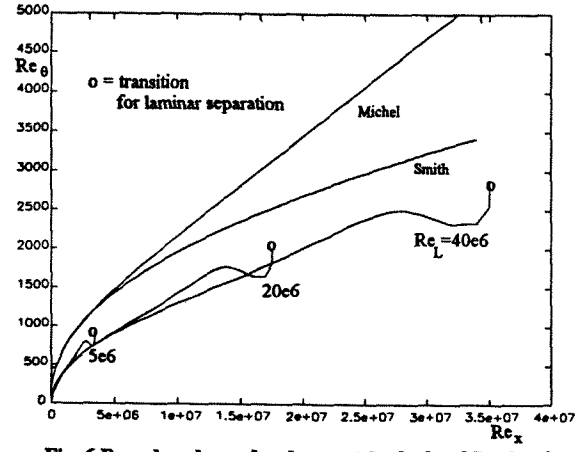

Fig. 6 Boundary layer development for body of fig. 4 and Michel/Smith transition prediction curves.

NLF body design optimization procedure

A computational design procedure has been developed to obtain extensive runs of laminar flow, in order to achieve lower drag coefficient for axisymmetric and three-dimensional bodies.
The numerical optimization method includes three elements : a constrained minimization program, a direct aerodynamic code (a solver to evaluate at each iteration the objective function that we want to minimize) and a parametric modification technique applied to the geometry. The computational design procedure used to obtain natural laminar flow bodies is described in the flow-chart presented in fig. 7.
As an optimizer, the constrained-minimization method proposed by Vanderplaats [16] has been used in the present investigation.
The objective function to be minimized is taken to be a function of a certain number of parameters :

$$F_{OBJ}=F(x_1, x_2, ...x_N) \qquad (2)$$

These parameters must satisfy some constraints conditions :

$$G_j(x_1,x_1,.....,x_1)\leq 0 \qquad j=1,..N_c \qquad (3)$$

and must be included in prescribed limits :

$$x_i^L < x_i < x_i^U \qquad i=1,...N \qquad (4)$$

The numerical optimization in aerodynamics has been used previously and tested by the authors for the optimization of mono and multi-component airfoils [17].
It was observed, and it will be re-stated in this work, that a good choice of the geometric parameters is imperative in order to obtain good optimization results. It is important to chose parameters which the objective function is more sensitive to.
Furthermore, it is important to choose the correct number of parameters for geometric representation because there must be sufficient numbers to allow significant shape modifications. An excess number of parameters could render obtaining the desired results infeasible.
It is important to note that it is of fundamental importance to introduce and control both geometric and aerodynamic constraints for the problem under consideration. This will help to avoid obtaining unsatisfactory solutions and will force the optimizer to achieve good solutions. The selection of pertinent parameters requires superior knowledge of the physical problem by the designer.

Results of axialsymmetric bodies design

Designing minimum drag axialsymmetric bodies is a common problem for hydronautic applications and in

some cases for glider fuselages or tip tanks in the aeronautical field.

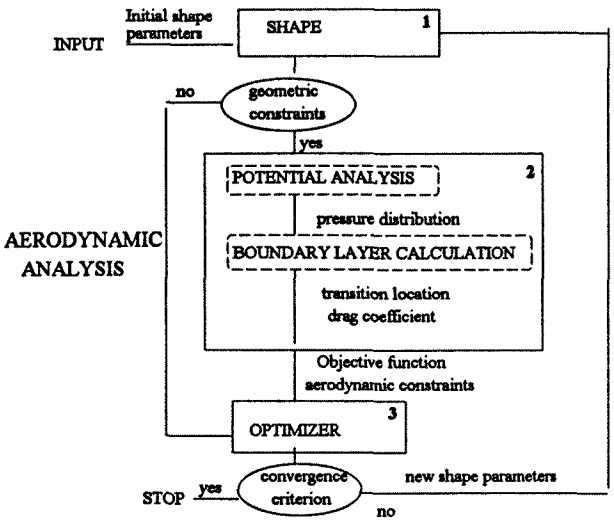

Fig. 7 Flowchart of design iterative procedure for NLF fuselage.

A preliminary check of validity of aerodynamic analysis has been made for an axialsymmetric body proposed in ref. 18 at various Reynolds numbers.
The geometry and the pressure distribution of this low drag axialsymmetric body is shown in fig. 8.
The body presents, at "low" Reynolds numbers (Re_L up to 20 million) a transition location immediately after the pressure peak.
Fig. 9 and 10 show the transition location and the drag coefficient based on maximum frontal area, varying the Reynolds number.
For Re_L less than 9 million the transition location numerically evaluated is fixed at the pressure peak location and the drag coefficient decreases with Re_L because the boundary layer becomes more thinner.
For Re_L greater than 20 million the laminar boundary layer becomes more unstable and the transition location moves toward the leading edge.
Due to the laminar flow extent reduction, the drag coefficient C_D begins to increase and it reachs a maximum value when the transition is located near the leading edge.
For greater Reynolds numbers, the drag coefficient slowly decreases due to the effect of viscous stresses that now play a lesser role with respect to inertial forces.
It is possible to define, for every slender body, a Reynolds number range in which there is no effect on the transition location (fixed approximately at the maximum thickness location) and a range in which the transition location is strongly effected even by a small variation of the Reynolds number value (the transition location in this condition is mainly influenced by the shape of the pressure distribution and not by the pressure peak location).

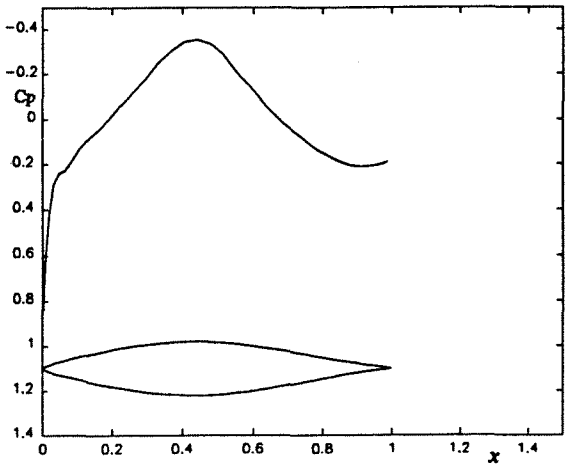

Fig. 8 Pressure distribution on F57 body of revolution (ref. 18)

A comparison with experimental data [19] for an axialsymmetric body tested in water up to a Reynolds number of about 16 million, shows agreement between numerical and experimental values (fig. 11).
There is uncertainty about the transition location at high Reynolds numbers ($Re_L \approx 40$ million) and no experimental data is available to suggest how much the laminar flow extension is influenced by high values of Reynolds number.
The geometric parametrization used to represent axialsymmetric bodies is the same adopted by Parson and Goodson [5] . The body of revolution is described by seven parameters, and the fineness ratio *fr*.
One of the most important parameters is the location of maximum thickness x_m , that strongly influences the transition location at low Reynolds numbers.

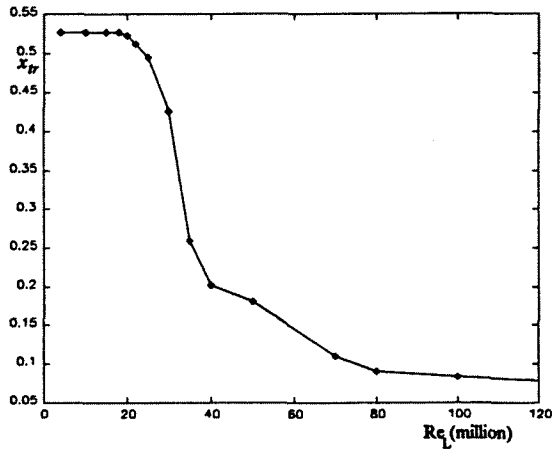

Fig. 9 Predicted transition location for F57 body of revolution (ref.18)

Starting from an initial configuration which present a fineness ratio of 5.0 and a x_m value of about 0.5 , drag optimization has been realized. This occurred through

larger extensions of natural laminar flow, in two Reynolds number conditions, i.e. for Re_L=4e6 and for Re_L=40e6.

The fineness ratio *fr* in the optimization process was fixed and geometric and aerodynamic constraints were imposed. In particular the maximum thickness location x_m was limited to the value of 0.8 (to avoid blunt trailing edge shapes) and completely attached flow was imposed at the trailing edge (x_{sep} >.95).

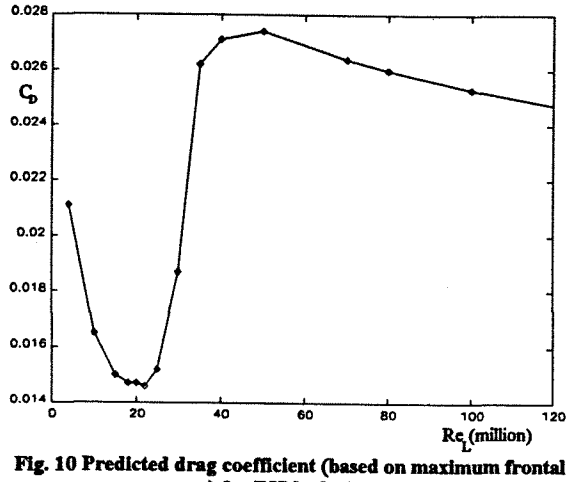

Fig. 10 Predicted drag coefficient (based on maximum frontal area) for F57 body (ref. 18)

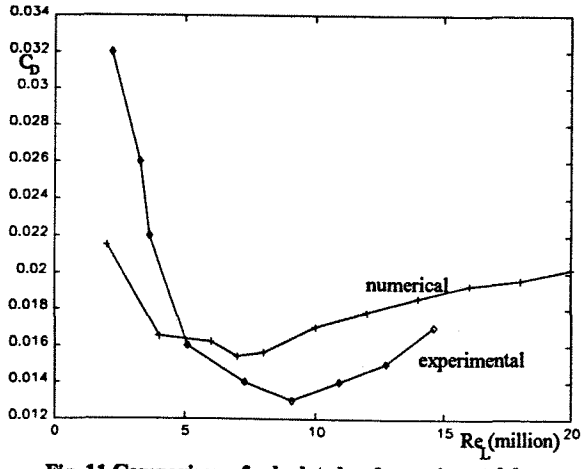

Fig. 11 Comparison of calculated and experimental drag coefficients for Hansen & Hoyt body (*fr*=4.5) (ref. 11).

At Re_L=4e6 the code provides a larger extension of laminar flow than the original body and a drag reduction moving the location of maximum thickness toward the trailing edge. In this way a larger favourable pressure gradient zone is obtained (fig. 12). The transition location moves from x_{tr}=.60 to x_{tr}=.76 and the drag coefficient based on maximum frontal area is reduced by about 15% (from 0.0206 to 0.0180). Fig. 13 shows the distribution of the amplification factor *n* for the two configurations. It can be seen that a stronger favourable pressure gradient delays the location at which the amplification of disturbances begins inside the boundary layer (*n* >0).

The optimization of the same initial shape at a Reynolds number of 40 million, shows interesting results.

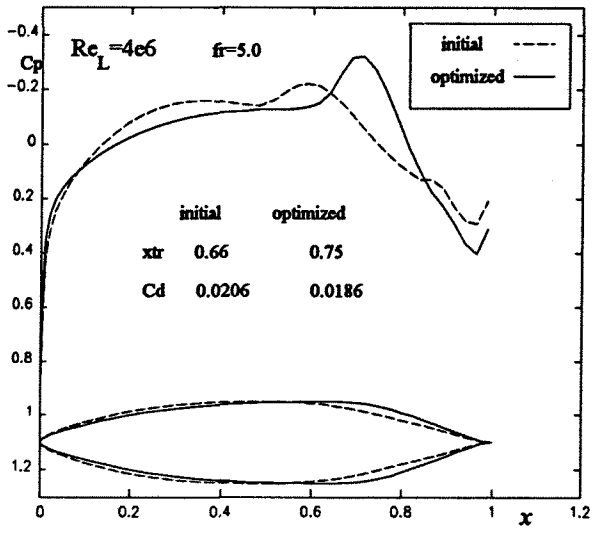

Fig. 12 Axialsymmetric drag optimization - Re_L=4e6 - geometry and pressure distribution for initial and optimized shape.

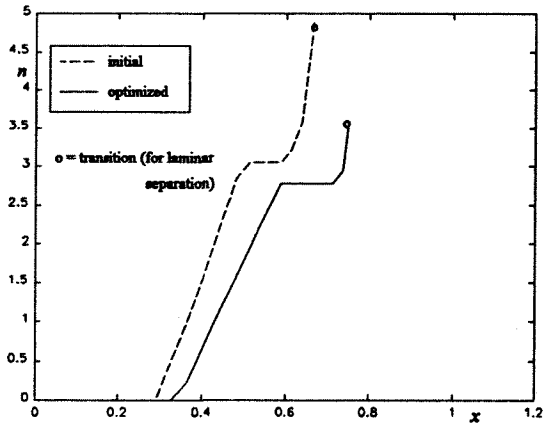

Fig. 13 Logarithmic disturbance amplification factor growth for initial and optimized shape at Re_L=4e6

To obtain more conservative results, and to take into account greater instability of axialsymmetric boundary layers, the value of *n*, at which transition is thought to take place, is set at 6 instead of at 9.

For the initial shape, at this Re_L condition, the transition location is x_{tr}= 0.23 and the drag coefficient is C_D=0.035.

The optimized shape presents a pressure distribution with a peak closer to the leading edge than that predicted for the initial shape (see fig. 14).

The different growth of *n* for the two shapes (fig. 15) shows that the different curvature of the pressure distribution delays the growth of *n* at higher values of *x*.

The transition location for the optimized shape is x_{tr}=0.32 and the drag coefficient is C_D=0.024, showing a reduction of about 30%.

It is clear that at this high Reynolds number condition, the curvature and the shape of the pressure distribution

along the forebody , influences the transition location more than the maximum thickness location (the flow is not able to remain laminar up to the peak).

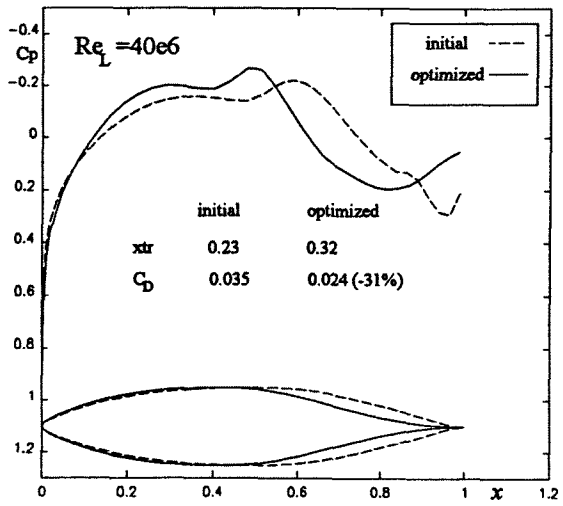

Fig. 14 Axialsymmetric drag optimization - Re_L=40e6 - geometries and pressure distribution for initial and optimized shape.

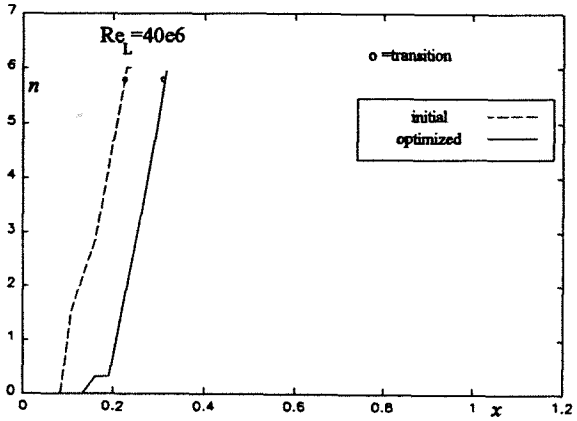

Fig. 15 Logarithmic disturbance amplification factor growth for initial and optimized shape at Re_L=40e6

Results of Three-Dimensional Fuselages Design

With the aerodynamic analysis technique previously described, we have done a preliminary drag calculation for two different fuselage shapes to estimate the influence of the forebody.

The two shapes tested are a conventional transport aircraft fuselage and a business aircraft fuselage (PIAGGIO P180).

Figg. 16 and 17 show the pressure distribution along the top and the bottom surface for the two fuselages.

The transition location on the top is x_{tr}=.16 for the conventional transport fuselage and x_{tr}=.33 for the business aircraft fuselage. The business aircraft fuselage shape presents a smoother and longer favourable pressure gradient.

In table 3 transition locations and drag coefficients for the two fuselages are shown.

The business aircraft fuselage presents a drag coefficient of 0.043, with respect to the value of 0.054 relative to the transport aircraft fuselage.

The equivalent area, indicated by f (product of drag coefficient for nondimensional maximum frontal area) is 20% lower for the business aircraft fuselage.

Figg. 18 and 19 show the pressure and the skin friction coefficient distribution around the two fuselages.

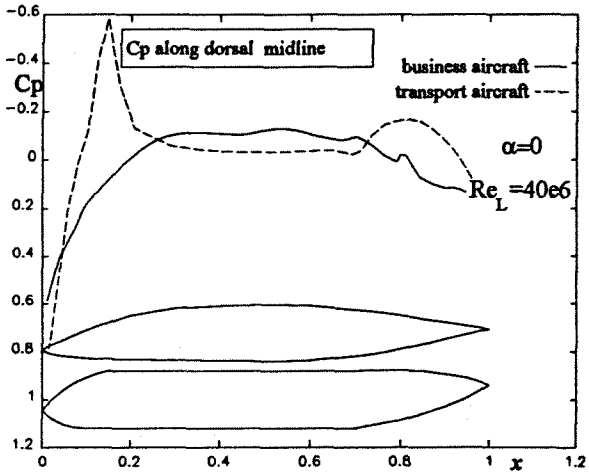

Fig. 16 Pressure distribution on dorsal midline for a business aircraft fuselage (PIAGGIO P180) and a transport aircraft fuselage

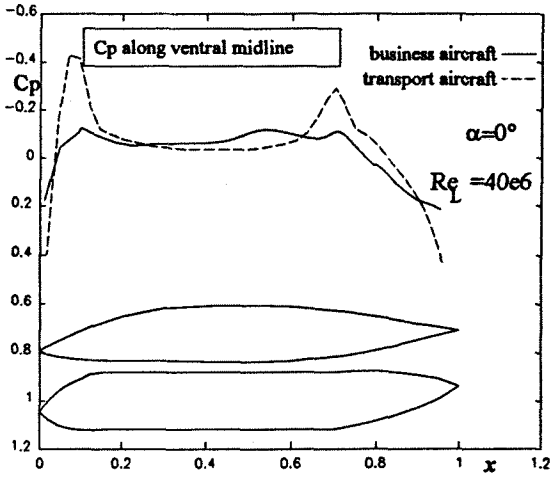

Fig. 17 Pressure distribution on ventral midline for a business aircraft fuselage (PIAGGIO P180) and a transport aircraft fuselage

To set up an iterative computational procedure, to design three-dimensional fuselage shapes, we had to solve the problem of the parameterization of such shapes. The problem is to represent a modification of an initial shape with a limited number of parameters.

By using a parameterization shape relative to the airfoil shape modification [20] , that is based on the Legendre polinomials equation, it is possible to establish a parametric dependence by using 6

parameters for each of the following functions: $K_u(x)$, $K_l(x)$, $K_y(x)$.
$K_u(x)$ is used for the upper surface modification, $K_l(x)$ for the lower surface modification, and $K_y(x)$ for the lateral variation of each fuselage section.
Through these 18 parameters, it is then possible to obtain a modification for each section as shown in fig. 20. The advantages of the parameterization are the low number of parameters and the homotopic section modification.
The results clearly show that this kind of parametric modification is particularly efficient for fuselages, because it permits preservation of the characteristics of the original shape.

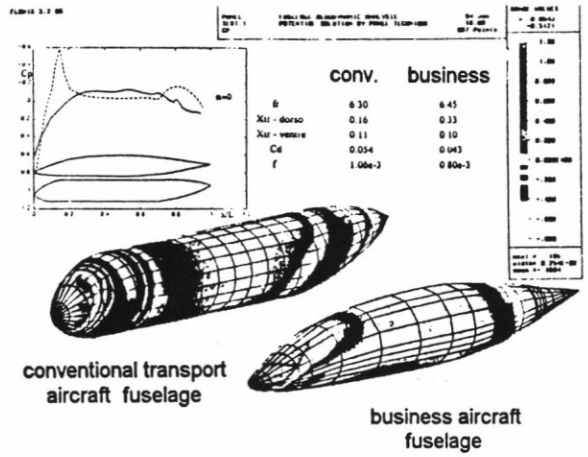

Fig. 18 Pressure distribution on business aircraft fuselage and conventional transoport aircraft fuselage - Re_L=40e6

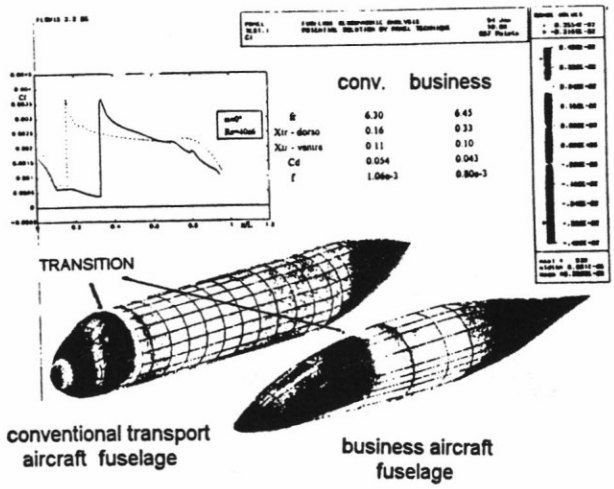

Fig. 19 Skin friction coefficient distribution on business aircraft fuselage and conventional transport aircraft fuselage - Re_L=40e6

α=0° Re_l=40e6

	fr	xtr up	xtr low	C_D up	C_D low	C_D TOT	$f \cdot 10^3$
business	6.45	0.33	0.10	0.039	0.046	0.044	0.803
transport	6.30	0.16	0.11	0.052	0.055	0.054	1.060

Table 3 Geometrics and aerodynamics characteristics for business aircraft fuselage and transport aircraft fuselage.

A drag optimization of the conventional transport fuselage has been done with the parametric modification technique illustrated above.

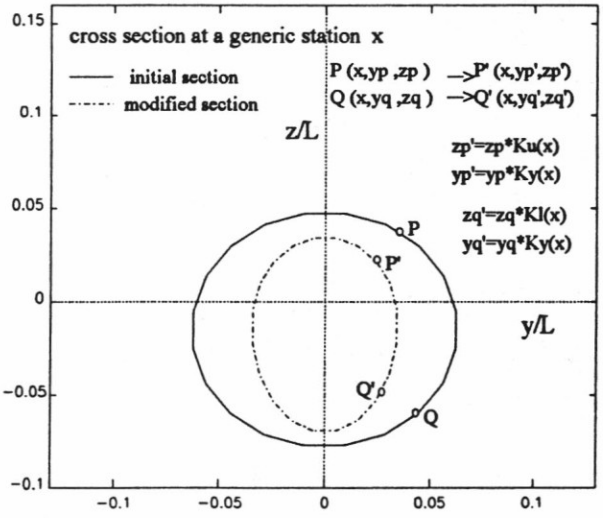

Fig. 20 Cross section shape modification technique

Initially no geometric constraints were imposed on the fuselage's shape (for example, maximum fineness ratio).
The code found a shape with a greater laminar flow extension, but with a greater maximum frontal area (fig. 21). The result is that the drag of the optimized fuselage is greater than that of the initial shape.
A new optimization was performed with a constraint on the fineness ratio, attempting to increase the natural laminar flow area. As it is shown in fig. 22, the shape modification in the forebody region done by the code led to a lower pressure peak level and a larger favourable pressure gradient.
The effect is that transition takes place at x_{tr}=0.24 instead of at x_{tr}=0.16 (initial shape).
A drag reduction of about 6% was obtained. Table 4 illustrates geometric and aerodynamic characteristics of the two fuselages. Fig. 23 shows the section modification performed by the code at two stations (x=0.075 and x=0.30).

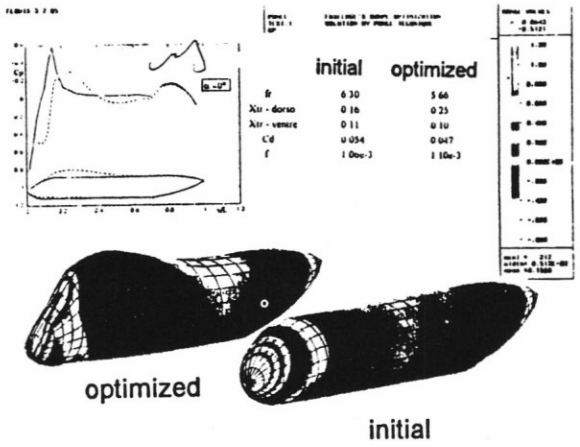

Fig. 21 Pressure distribution for initial and optimized fuselage, no geometric constraints imposed in the optimization process.

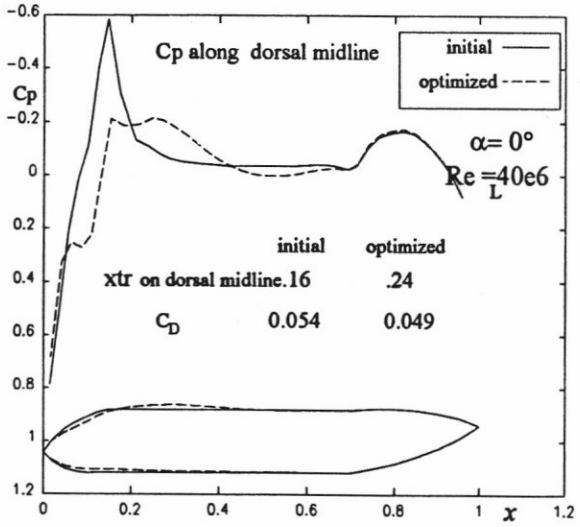

Fig. 22 Fuselage drag optimization, Re_L=40e6, pressure distribution along dorsal midline for initial and optimized shape

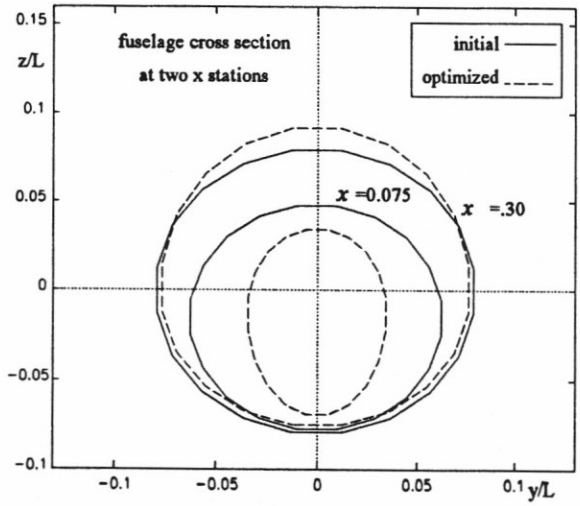

Fig. 23 Fuselage cross section of initial and optimized shape at two longitudinal stations.

α=0° Re_L=40e6

	fr	xtr up	xtr low	C_D up	C_D low	C_D TOT	$f \cdot 10^3$
initial	6.30	0.16	0.11	0.052	0.055	0.054	1.060
optimized	6.15	0.24	0.11	0.047	0.052	0.049	0.990

Table 4 Geometric and aerodynamic characteristics of initial and optimized aircraft fuselage

In the first forebody the section has been reduced, especially in the horizontal direction, trying to obtain a "fish-head" shape.

Figg. 24 and 25 show three-dimensional shape, pressure and skin friction distibution for the initial and the optimized fuselage.

A typical run that requires about 400 iterations, using 500 surface panels took about 30 seconds per iteration of a CONVEX 34 cpu time.

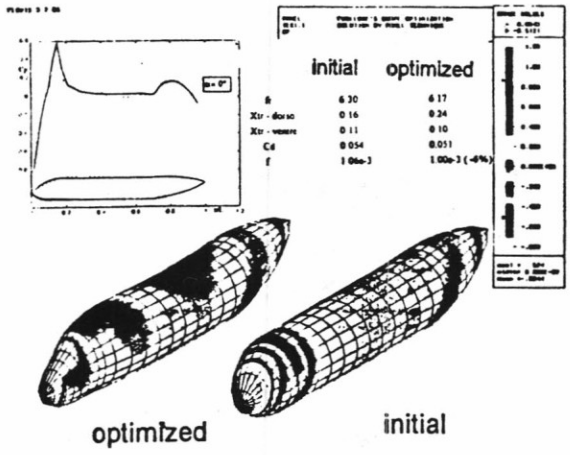

Fig. 24 Pressure distribution on initial and optimized conventional transport aircraft fuselage.

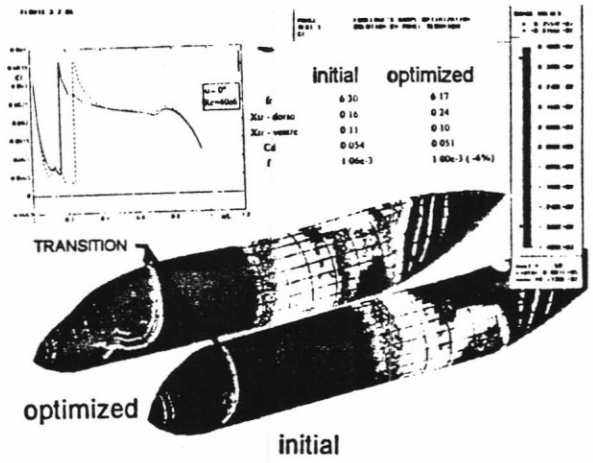

Fig. 25 Skin friction coefficient distribution on initial and optimized conventional transport aircraft fuselage.

Conclusions

A numerical optimization procedure, to design axialsymmetric and three-dimensional bodies, characterized by large areas of Natural Laminar Flow, has been developed.

The code is completely modular, in that it is easy to change a module and address a different problem (for example two-dimensional multi-component airfoils design). Upon investigating existing transition prediction methods, we found the current methods are sufficient for a limited range of Reynolds numbers. However, existing methods were not adequate or accurate predictors for higher Reynolds numbers.

Furthermore, there is a lack of existing experimental data obtained in this high Reynolds numbers range (30 ÷70 million) to modify current transition methods.

Sensitivity of the methods to the choice of the objective function and constraints has been highlighted.

Furthermore, we have proposed an extension of the existing optimization procedures to general 3D fuselages.

In doing this, a way to parametrize the geometry of a three-dimensional body has been suggested.

Presented are results of an optimization process, showing drag reduction up to 20% and an increase in the transition location.

Due to the pratical difficulties in maintaining Natural Laminar Flow along fuselages, the extension of this work for the inclusion of Laminar Flow Control (LFC) technique is under consideration.

Aknowledgment

The authors are grateful to Mrs. Barbara Parson for her help in writing this work.

References

[1] Somers D.M., 1981, Design and Experimental Results for a Natural Laminar Flow Airfoil for General Aviation Application, NASA TP 1861

[2] Dodbele, S. S., van Dam, C. P., and Vijgen, P., "Design of Fuselage Shapes for Natural Laminar Flow," NASA CR-3970, March 1986.

[3] Dodbele, S. S., Van Dam, C. P., Vijgen, P. M. H. W., and Holmes, B. J., "Shaping of Airplane Fuselages for Minimum Drag," *Journal of Aircraft*, Vol. 24, No. 5, May 1987, pp. 298-304.

[4] Dalton, C. and Zedan, M. F., "Design of Low Drag Axisymmetric Shapes by the Inverse Method," *Journal of Hydronautics*, Vol. 15, Jan.-Dec., 1981, pp. 48-54.

[5] Parson, J. S., Goodson, R. E., and Goldchmied, F. R. ,"Shaping of Axisymmetric Bodies for Minimum Drag in Incompressible Flow," *Journal of Hydronautics*, Vol. 8, July 1974, pp. 100-107.

[6] Nicolosi, F., "Design Aerodinamico Bidimensionale e Tridimensionale tramite Ottimizzazione Numerica," Graduation Thesis, Univ. of Naples, February 1994

[7] von Karman, T., "Calculation of the Flowfield around Airships," NACA TM 574, July 1930.

[8] Hess, J. L., "The Unsuitability of Ellipsoids as Test Cases for Line-Source Methods," *Journal of Aircraft*, Vol. 22, April 1985, pp. 364-367

[9] Hess, J. , Smith, A.M.O. , "Calculation of non Lifting Potential Flow about arbitrary Three Dimensional Bodies," DOUGLAS report ES40622

[10] Drela, M. , "Two-Dimensional Transonic Aerodynamic Design and Analysis using the Euler Equations," GTL report n. 187, 1986

[11] Young,A. D., "The Calculation of Total and Skin Friction Drag of Bodies of Revolution at Zero Incidence," ARC R&M 1874, April 1939

[12] Michel, R., "Etude de la Transition sur les Profils d'aile-Establissement d'un Point de Transition et Calcul de la Trainee de profil en Incompressible," ONERA, Rapport 1/1758A, 1951.

[13] Smith, A. M. O. and Gamberoni, H., "Transition, Pressure Gradient and Stability Theory," Douglas Aircraft Company, Long Beach, Calif., Rept ES26388, 1956

[14] Wazzan, A. R., Gazley C. and Smith, A. M. O.,"H-R_x Method for Predicting Transition," *AIAA Journal*, Vol. 19, June 1981, pp. 810-812

[15] Eppler, R. "Recent Developments in Boundary Layer Computation," *International Conference on Aerodynamics at Low Reynolds Numbers*, Vol. II, Royal Aeronautical Society, London, October 1986

[16] Vanderplaats, G. N. ,"Numerical Optimization Techniques for Engineering design : With Applications," ,Mc. Graw-Hill Book Company, 1984

[17] Coiro, D.P. , Nicolosi, F., "Design through Numerical Optimization of a Multi-Component high-lift Device," - February 1994 - To be Published.

[18] Parson, J. S. and Goodson, R. E., "The Optimum Shaping of Axisymmetric Bodies for Minimum Drag in Incompressible Flow," Purdue Univ., Rept ACC-72-6, June 1972.

[19] Hansen, R. J. and Hoyt, J. G., "Laminar-to-Turbulent Transition on a Body of Revolution with an Extended Favourable Pressure Gradient Forebody," *Transactions of the ASME*, Vol. 106, June 1984, pp. 202-210.

[20] Renaux, J., "Méthode de Définition de Profils par Optimisation Numérique," La Recherche Aérospatiale, 1984, n. 5 , pp 303-321